Supporting Information for Publication

Two Faces of Water in the Formation and Stabilization of Multicomponent Crystals of Zwitterionic Drug-Like Compounds

Artem O. Surov [1], **Nikita A. Vasilev** [1], **Andrei V. Churakov** [2], **Olga D. Parashchuk** [3], **Sergei V. Artobolevskii** [4],
Oleg A. Alatortsev [4], **Denis E. Makhrov** [4] **and Mikhail V. Vener** [2,4,*]

[1] G.A. Krestov Institute of Solution Chemistry of RAS, Ivanovo 153045 Russia; aos@isc-ras.ru (A.O.S.); nav@isc-ras.ru (N.A.V.)
[2] N.S. Kurnakov Institute of General and Inorganic Chemistry of RAS, Moscow 119991, Russia; churakov@igic.ras.ru
[3] Faculty of Physics, Lomonosov Moscow State University, Moscow 119991, Russia; olga_par@physics.msu.ru
[4] Department of Quantum Chemistry, D. Mendeleev University of Chemical Technology, Moscow 125047, Russia; Artobolevskiy_Sergey_Vladimirovich@muctr.ru (S.V.A.); Olegalatorcev@muctr.ru (O.A.A.); Denis_Makhrov@muctr.ru (D.E.M.)
[*] Correspondence: venermv@muctr.ru

Table of Contents:

S1. Periodic (Solid-state) DFT Calculations Followed by Bader Analysis of the Crystalline Electron Density

Periodic DFT computations with all-electron Gaussian-type orbitals were performed using Crystal17 [1]. The tolerance on energy controlling the self-consistent field convergence for geometry optimizations and frequency computations was set to 10^{-10} and to 10^{-11} Hartree, respectively. The number of points in the numerical first-derivative calculation of the analytic nuclear gradients equals 2. The shrinking factor reflecting the density of the k-points grid in the reciprocal space was set to 3. *K*-space sampling was limited to the   point. Raman intensities were calculated using the "RAMANEXP" keyword. Temperature was 298 K, the frequency of the incoming laser was 633 nM.

Experimental crystal structures of [2AmNic+Fum+H_2O] (1:1:1) and [2AmNic+Mle+H_2O] (1:1:1) (this work) and fumaric acid (Refcode FUMAAC) were used as input for all geometry optimization computations, with hydrogen atom positions normalized to standard neutron diffraction values.

All crystals structures optimized at the B3LYP/6-31G** level were found to correspond to the minimum point on the potential energy surface. The crystals structures of [2AmNic+Fum+H_2O] (1:1:1) and fumaric acid optimized at the PBE-D3/6-31G** level were found to correspond to the minimum point on the potential energy surface, while the imaginary frequency was found for crystalline [2AmNic+Mle+H_2O] (1:1:1).

Bader analysis of crystalline electron density was performed in the TOPOND software [2] currently built into CRYSTAL suit. The search for (3;-1) critical points was conducted between the pairs of atoms within the 5Å radius, and the interactions with electron density ρ_b in the (3;-1) point higher than 0.003 a.u. were taken for consideration.

Table S1. Theoretical values of the enthalpy, ΔH_{HB}, and energy, E_{HB}, of intermolecular H-bonds in the [2AmNic+Fum+H_2O] (1:1:1) crystal evaluated using several empirical approaches. The O⋯H distances, frequencies of the OH stretching vibrations and crystalline electron density were calculated using periodic DFT computations at the B3LYP/6-31G** level. The $\Delta H_{HB}/E_{HB}$ values, obtained using R(O⋯H), $\Delta\nu$ and G_b computed at the PBE-D3/6-31G** level are indicated in parentheses.

| Fragment [1]	R(O⋯H), Å	$-\Delta H_{HB}$ [2], kJ/mol	$-\Delta H_{HB}$ [3], kJ/mol	E_{HB} [4], kJ/mol
O12…H21-N2	1.840 (1.810)	23.4 (24.6)	-	26.8 (30.0)
O11…H11-N1	1.628 (1.599)	34.0 (36.0)	-	45.7 (48.0)
O12…H31-O3	1.709 (1.683)	29.3 (30.7)	27.8 (31.0)	35.8 (37.5)
O13…H32-O3	2.034 (1.819)	17.2 (24.3)	18.3 (21.9)	24.3 (26.1)
O11…H14-O14	1.563 (1.542)	38.5 (40.1)	39.7 (41.8)	52.9 (54.6)
O3…H1-O1	1.571 (1.520)	37.9 (41.9)	40.7 (44.4)	52.1 (57.9)

[1] the atomic numbering is given in Figures 1 and 2;

[2] evaluated using the Rozenberg approach [3]: $-\Delta H_{HB}$ [kJ mol^{-1}] = 0.134·R(O⋯H) $^{-3.05}$, where the R(H⋯O) is the H⋯O distance (nm);

[3] evaluated using the Iogansen approach [4]: $-\Delta H_{HB}$ [kJ mol^{-1}] = 1.386·($\Delta\nu$ [cm^{-1}] – 40)$^{0.5}$, where $\Delta\nu = \nu$(OH$_{free}$) – ν(OH) represents the red-shift value of the OH stretching frequency caused by the formation of the H-bond with the OH group being the proton donor. It should be noted that ν(OH$_{free}$) and ν(OH) are the frequencies of the localized, uncoupled OH stretching vibration;

[4] evaluated using the Espinoza approach [5]: E_{HB} [kJ mol^{-1}] = 1124·G_b [atomic units], where G_b is the positively-defined local electronic kinetic energy density at the O⋯H bond critical point.
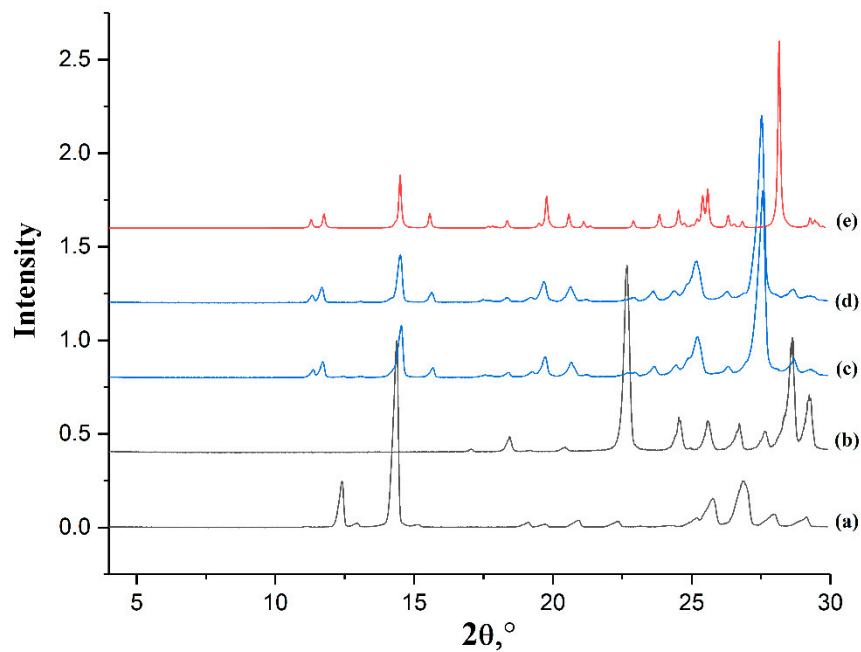
Figure S1. Experimental PXRD patterns of 2-aminonicotinic acid (a), fumaric acid (b), [2AmNic+Fum+H$_2$O] (1:1:1) salt prepared by liquid-assisted grinding (c) and slurry (d) and PXRD patterns calculated from the single crystal diffraction data for [2AmNic+Fum+H$_2$O] (1:1:1) (e).
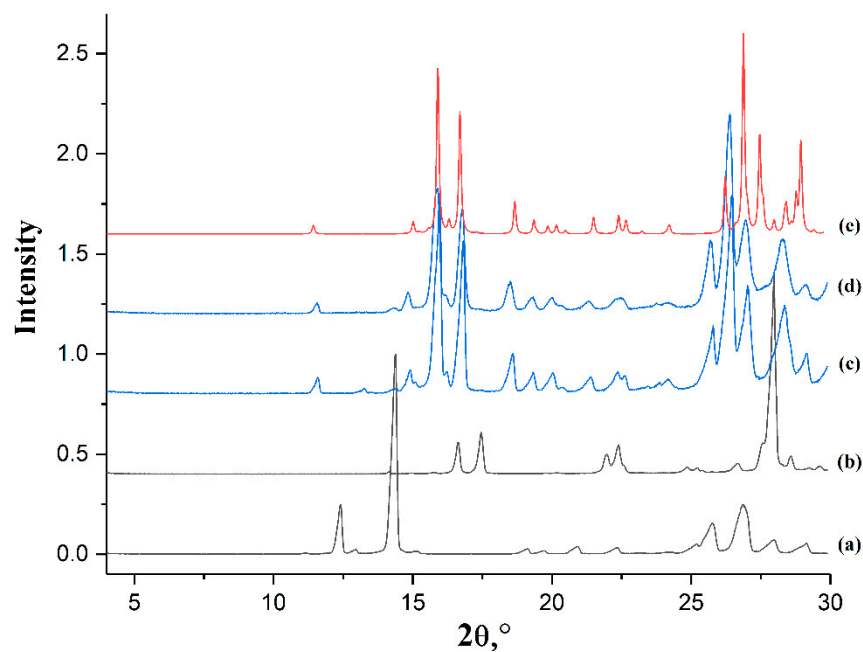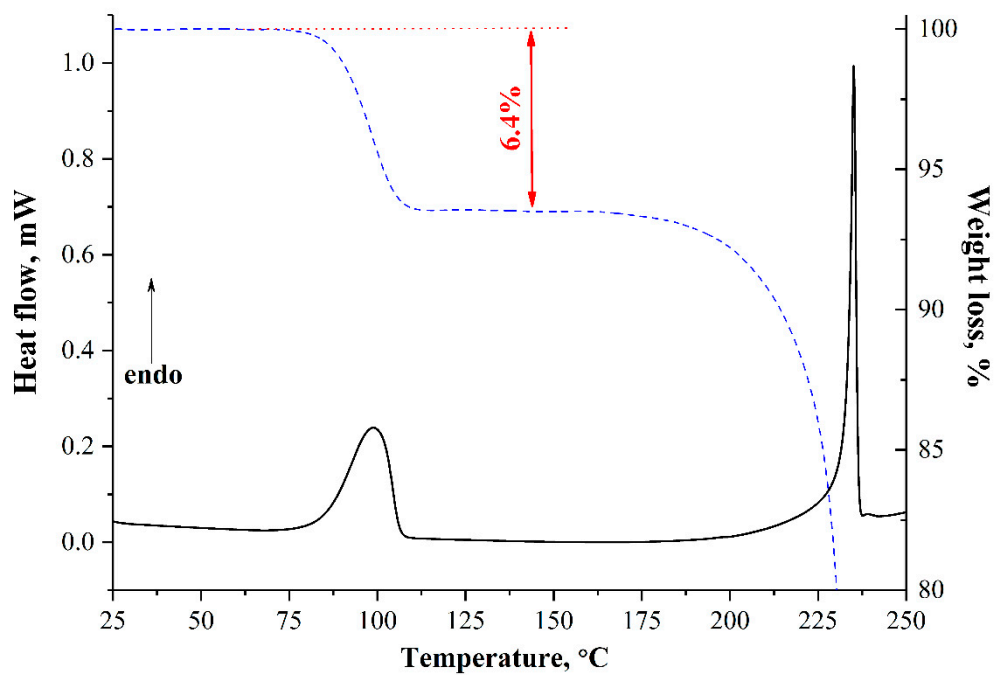

Figure S2. Experimental PXRD patterns of 2-aminonicotinic acid (a), maleic acid (b), [2AmNic+Mle+H$_2$O] (1:1:1) salt prepared by liquid-assisted grinding (c) and slurry (d) and PXRD patterns calculated from the single crystal diffraction data for [2AmNic+Mle+H$_2$O] (1:1:1) (e).

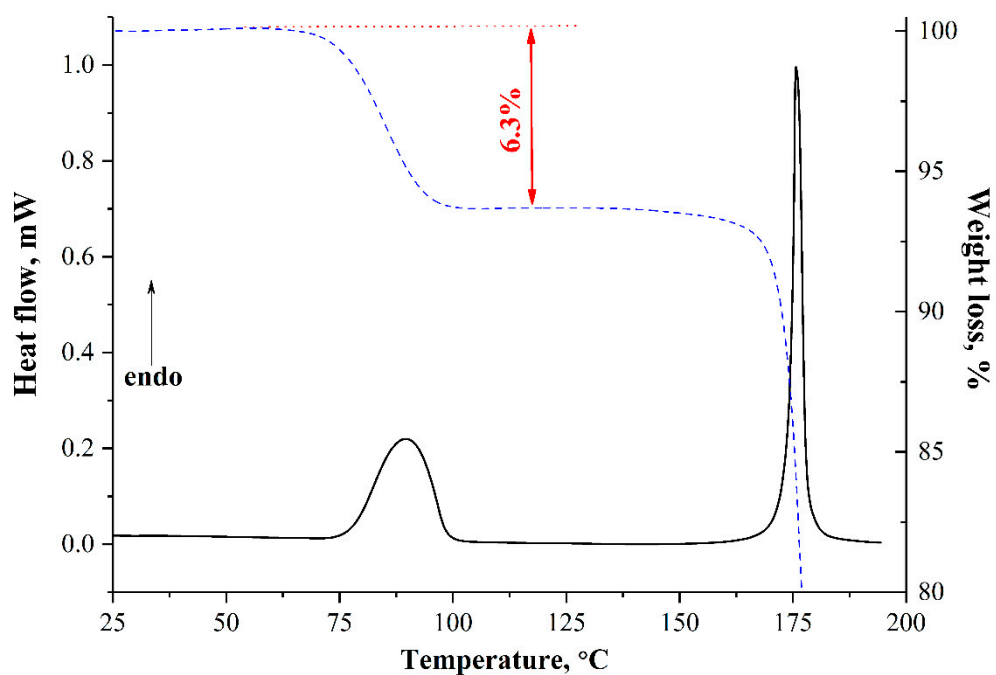**Figure S3.** Results of DSC/TG analyses of [2AmNic+Fum+H$_2$O] (1:1:1).
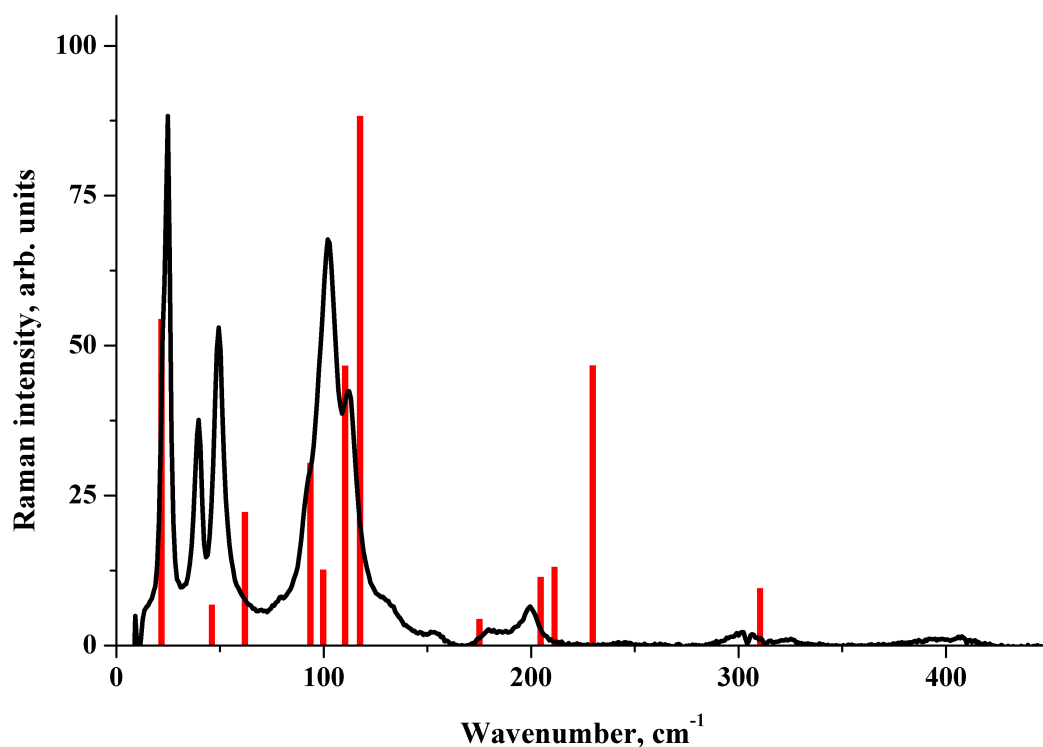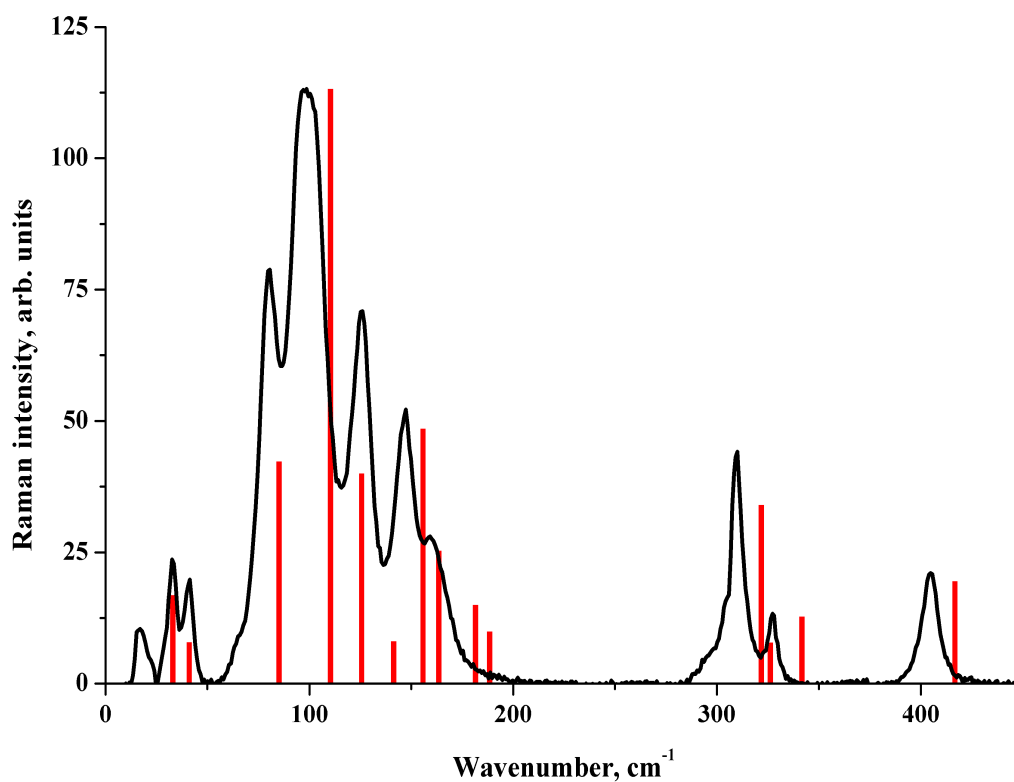

Figure S4. Results of DSC/TG analyses of [2AmNic+Mle+H$_2$O] (1:1:1).

Figure S5. Raman spectrum of the [2AmNic+Fum+H₂O] (1:1:1) crystal. Experiment (black line) vs. B3LYP/6-31G** computations (red bars). The height of the bars is proportional to the relative Raman intensity of the corresponding transition.


Figure S6. Raman spectrum of the [2AmNic+Mle+H₂O] (1:1:1) crystal. Experiment (black line) vs. B3LYP/6-31G** computations (red bars). The height of the bars is proportional to the relative Raman intensity of the corresponding transition.
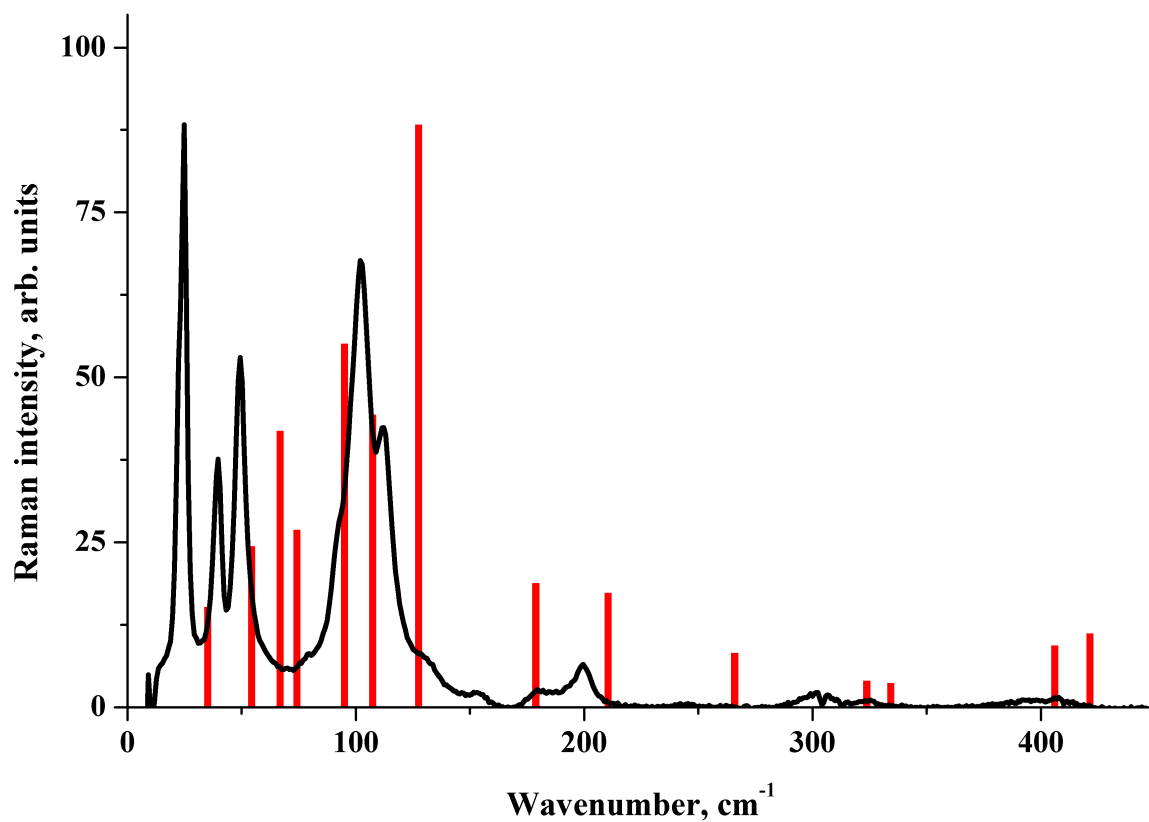
Figure S7. Raman spectrum of crystalline fumaric acid. Experiment (black line) vs. B3LYP/6-31G** computations (red bars). The height of the bars is proportional to the relative Raman intensity of the corresponding transition.
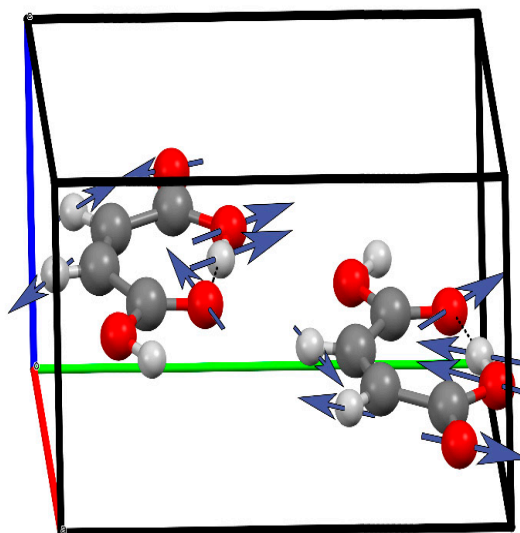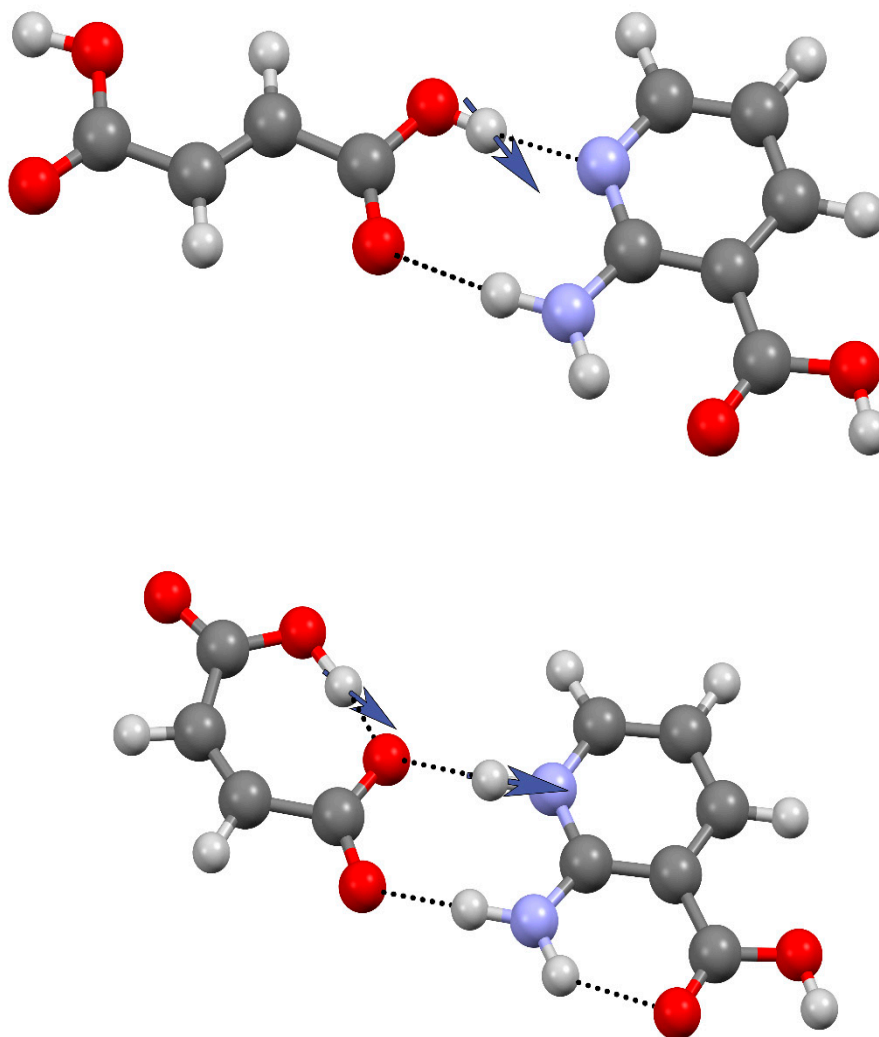

Figure S8. Schematic representation of Raman active vibration of 337 cm^{-1} of crystalline maleic acid, evaluated using periodic DFT computations at the B3LYP/6-31G** level. Arrows indicate directions of relative atom displacements.

Figure S9. Schematic representation of the IR active vibration of 2524 cm^{-1} of the fumaric acid-2-amino-nicotinic acid zwitterion heterodimer (**upper panel**) and 2636 cm^{-1} of the maleic acid-2-amino-nicotinic acid zwitterion (**lower panel**), evaluated using DFT computations at the B3LYP/6-31G** level. Arrows indicate directions of relative atom displacements.

Table S2. Crystallographic data for [2AmNic+Fum+H_2O] (1:1:1) and [2AmNic+Mle+H_2O] (1:1:1) multicomponent crystals.

Chemical formula	[2AmNic+Fum+H_2O] (1:1:1) $C_6H_7N_2O_2 \cdot C_4H_3O_4 \cdot H_2O$	[2AmNic+Mle+H_2O] (1:1:1) $C_6H_7N_2O_2 \cdot C_4H_3O_4 \cdot H_2O$
M_r	272.22	272.22
Crystal system, space group	Monoclinic, $P2_1/n$	Monoclinic, $C2/c$
Temperature (K)	150	150
a, b, c (Å)	9.8337 (3), 11.2338 (3), 10.5614 (2)	31.6781 (8), 6.7294 (2), 11.4707 (3)
β (°)	90.974 (1)	107.0322 (9)
V (Å^3)	1166.55 (5)	2338.01 (11)
Z	4	8
Radiation type	Mo $K\alpha$	Mo $K\alpha$
μ (mm^{-1})	0.13	0.13
Crystal size (mm)	0.45 × 0.40 × 0.25	0.45 × 0.30 × 0.01
Data collection		
Diffractometer	Bruker *SMART APEX* II	Bruker *SMART APEX* II
Absorption correction	Multi-scan *SADABS* (Bruker, 2016)	Multi-scan *SADABS* (Bruker, 2016)
No. of measured, independent and observed [$I > 2\sigma(I)$] reflections	13319, 3097, 2648	18047, 2553, 2187
R_{int}	0.027	0.031
$(\sin \theta/\lambda)_{max}$ (Å^{-1})	0.682	0.639
Refinement		
$R[F^2 > 2\sigma(F^2)]$, $wR(F^2)$, S	0.041, 0.103, 1.07	0.035, 0.087, 1.06
No. of reflections	3097	2553
No. of parameters	220	220
H-atom treatment	All H-atom parameters refined	All H-atom parameters refined
$\Delta\varrho_{max}$, $\Delta\varrho_{min}$ (e Å^{-3})	0.44, −0.25	0.29, −0.16

References

1. Dovesi, R.; Erba, A.; Orlando, R.; Zicovich-Wilson, C.M.; Civalleri, B.; Maschio, L.; Rérat, M.; Casassa, S.; Baima, J.; Salustro, S.; et al. Quantum-mechanical condensed matter simulations with CRYSTAL. *WIREs Comput. Mol. Sci.* **2018**, *8*, e1360, doi:10.1002/wcms.1360.
2. Gatti, C.; Saunders, V.R.; Roetti, C. Crystal field effects on the topological properties of the electron density in molecular crystals: The case of urea. *J. Chem. Phys.* **1994**, *101*, 10686–10696.
3. Rozenberg, M.; Loewenschuss, A.; Marcus, Y. An empirical correlation between stretching vibration redshift and hydrogen bond length. *PCCP* **2000**, *2*, 2699–2702, doi:10.1039/B002216K.
4. Iogansen, A.V. Direct proportionality of the hydrogen bonding energy and the intensification of the stretching ν(XH) vibration in infrared spectra. *Spectrochim. Acta Part A Mol. Biomol. Spectrosc.* **1999**, *55*, 1585–1612, doi:10.1016/S1386-1425(98)00348-5.
5. Mata, I.; Alkorta, I.; Espinosa, E.; Molins, E. Relationships between interaction energy, intermolecular distance and electron density properties in hydrogen bonded complexes under external electric fields. *Chem. Phys. Lett.* **2011**, *507*, 185–189, doi:10.1016/j.cplett.2011.03.055.
6. Tsirelson, V. G. *The Quantum Theory of Atoms in Molecules: From Solid State to DNA and Drug Design.* Eds: Matta, C.F. and Boyd, R.J. Wiley-VCH Verlag GmbH & Co. KGaA: Weinheim, Germany, 2007.